Temporal control of contact site formation reveals a relationship between mitochondrial division and Num1-mediated mitochondrial tethering

Clare S. Harper, Jason C. Casler, and Laura L. Lackner*
Department of Molecular Biosciences, Northwestern University, Evanston, IL, 60208

ABSTRACT **Mitochondrial division is critical for maintenance of mitochondrial morphology and cellular homeostasis. Previous studies have suggested that the mitochondria-ER-cortex anchor (MECA), a tripartite membrane contact site between mitochondria, the ER, and the plasma membrane, is involved in mitochondrial division. However, its role is poorly understood. We developed a system to control MECA formation and depletion, which allowed us to investigate the relationship between MECA-mediated contact sites and mitochondrial division. Num1 is the protein that mediates mitochondria-ER-plasma membrane tethering at MECA sites. Using both rapamycin-inducible dimerization and auxin-inducible degradation components coupled with Num1, we developed systems to temporally control the formation and depletion of the native contact site. Additionally, we designed a regulatable Num1-independant mitochondria-PM tether. We found that mitochondria-PM tethering alone is not sufficient to rescue mitochondrial division and that a specific feature of Num1-mediated tethering is required. This study demonstrates the utility of systems that regulate contact-site formation and depletion in studying the biological functions of membrane contact sites.**

Monitoring Editor
Martin Ott
University of Gothenburg

Received: May 15, 2023
Revised: Jul 17, 2023
Accepted: Aug 9, 2023

SIGNIFICANCE STATEMENT

- The mitochondria-ER-cortex anchor (MECA) forms a membrane tether between mitochondria, the endoplasmic reticulum, and the plasma membrane. Multiple functions have been attributed to MECA, including a poorly defined role in mitochondrial division.
- The authors developed systems to control the formation and depletion of the contact site. Using these tools, they found that mitochondrial tethering alone is not sufficient to rescue mitochondrial division and that a specific feature of MECA-mediated tethering is required.
- Regulatable contact sites, like those developed in this study, provide the ability to observe the downstream consequences of contact site formation and depletion in real time.

This article was published online ahead of print in MBoC in Press (http://www.molbiolcell.org/cgi/doi/10.1091/mbc.E23-05-0168) on August 16, 2023.

*Address correspondence to: Laura L. Lackner (Laura.Lackner@northwestern.edu).

Abbreviations used: AID, auxin-inducible degron; CC, coiled-coil; DMSO, dimethylsulfoxide; ER, endoplasmic reticulum; MCSs, membrane contact sites; MECA, mitochondria-ER-cortex anchor; PH, pleckstrin homology; PI[4,5]P2, phosphoinositide phosphatidylinositol 4,5-biophosphate; PM, plasma membrane; RID, rapamycin-induced dimerization; SCD, synthetic complete dextrose; SD, standard deviation; WT, wild-type; yEGFP, yeast enhanced GFP; YPD, yeast peptone dextrose.

INTRODUCTION

Having everything in the right place at the right time is vital for the complex coordination of cellular processes. Organelles are no exception to this, as the distribution of organelles is critical for cell health. For example, in budding yeast, several organelles need to be trafficked into the growing daughter cell and properly positioned in both the mother- and daughter-cell before cell division in order to ensure cell viability (Fagarasanu and Rachubinski, 2007; Eves *et al*., 2012; Knoblach and Rachubinski, 2015; Li *et al*., 2021). Organelle distribution is controlled by trafficking via motor proteins, organelle biogenesis, dynamics such as fission and fusion, and tethering to other membranes. Tethering takes place at membrane contact sites

(MCSs), or areas of close apposition between membranes without fusion (Scorrano *et al.*, 2019). MCSs are mediated by molecules that tether organelle membranes together through protein–protein or protein-lipid interactions. Sometimes tethering is brief and dynamic, such as with ER-Golgi contacts (David *et al.*, 2021). In other cases, MCSs are stable and robust. One such example is the *Saccharomyces cerevisiae* mitochondria-ER-cortex anchor (MECA), which forms a tripartite membrane tether between mitochondria, the endoplasmic reticulum (ER), and the plasma membrane (PM) that is stable throughout the cell cycle (Cerveny *et al.*, 2007; Tang *et al.*, 2012; Klecker *et al.*, 2013; Lackner *et al.*, 2013).

MECA is composed of Num1, a 313 kDa protein that interacts directly with the outer mitochondrial membrane through its N-terminal coiled-coil (CC) domain (Tang *et al.*, 2012; Lackner *et al.*, 2013; Ping *et al.*, 2016), and the PM through its C-terminal pleckstrin homology (PH) domain, which binds with high specificity to the PM-enriched phosphoinositide phosphatidylinositol 4,5-bisphosphate (PI[4,5]P2) (Yu *et al.*, 2004; Tang *et al.*, 2009). The association of Num1 with the ER is thought to be mediated by an interaction between Num1 and the integral ER membrane protein Scs2 (Chao *et al.*, 2014; Omer *et al.*, 2018; Figure 1A). The association between Num1 and mitochondria drives the assembly of Num1 into stable clusters that tether the three membranes together (Kraft and Lackner, 2017). When mitochondria are trafficked into the growing daughter cell, MECA-mediated mitochondrial tethering helps retain mitochondria in the mother cell (Cerveny *et al.*, 2007; Klecker *et al.*, 2013; Lackner *et al.*, 2013). Following mitochondrial inheritance, Num1 clusters form and tether mitochondria in the bud, ensuring mitochondria are maintained in the bud during cell division (Kraft and Lackner, 2017).

Similar to many MCS proteins, Num1 is multifunctional and has additional roles in the cell besides tethering organelles (Eisenberg-Bord *et al.*, 2016; Lackner, 2019; Scorrano *et al.*, 2019; Harper *et al.*, 2020; Prinz *et al.*, 2020). In addition to maintaining mitochondrial distribution during inheritance, Num1 is required for the function of dynein in nuclear inheritance. Dynein is trafficked to the plus ends of astral microtubules and offloaded onto Num1 clusters at the cortex. Num1-anchored dynein then captures and walks along astral microtubules, generating the force to align the mitotic spindle for nuclear inheritance (Kormanec *et al.*, 1991; Eshel *et al.*, 1993; Carminati and Stearns, 1997; Adames and Cooper, 2000; Heil-Chapdelaine *et al.*, 2000; Farkasovsky and Küntzel, 2001; Lammers and Markus, 2015). Interestingly, Num1-mediated dynein anchoring is also important for mitochondrial function; when dynein is unable to anchor at cortical Num1 clusters, defects in mitochondrial respiration are observed (White *et al.*, 2022). Thus, although MCS proteins have roles in seemingly distinct pathways, these roles may be interrelated in order to coordinate cellular processes.

In addition to its roles in mitochondrial tethering and dynein anchoring, Num1 has also been implicated in mitochondrial division (Cerveny *et al.*, 2007). Mitochondrial division and the opposing activity of mitochondrial fusion are critical for maintaining the shape and health of the mitochondrial network and the integrity of mitochondrial DNA (mtDNA; Hoppins *et al.*, 2007; Nunnari and Suomalainen, 2012; Osman *et al.*, 2015). The mechanisms of mitochondrial division and fusion are conserved from yeast to metazoa (Hoppins *et al.*, 2007). In yeast, the dynamin-related GTPase Dnm1 drives mitochondrial division. Dnm1 is recruited to the mitochondrial surface by the adaptor protein Mdv1, which binds to the outer mitochondrial membrane protein Fis1 (Mozdy *et al.*, 2000; Tieu and Nunnari, 2000; Cerveny *et al.*, 2001; Tieu *et al.*, 2002; Cerveny and Jensen, 2003). Mdv1 subsequently helps promote the assembly of Dnm1 into a helical structure that wraps around the organelle, causing constriction and ultimately scission of the mitochondrial membranes (Naylor *et al.*, 2006; Lackner *et al.*, 2009; Mears *et al.*, 2011). Num1 was identified in a genetic screen as a putative Dnm1-interacting protein and was suggested to be critical for mitochondrial division (Cerveny *et al.*, 2007). A subsequent study demonstrated that Num1 is not required for mitochondrial division, but that the rates of mitochondrial division are reduced in cells lacking Num1 (Lackner *et al.*, 2013). However, the mechanism by which Num1 impacts mitochondrial division is unclear. One hypothesis is that Num1-mediated tethering of mitochondria creates tension across the mitochondrial membrane as it is stretched between anchor points (Schauss and McBride, 2007; Lackner and Nunnari, 2009; Hammermeister *et al.*, 2010). Several studies suggest that membrane tension is important for the ability of dynamin-related proteins to mediate membrane scission (Roux *et al.*, 2006; Mahecic *et al.*, 2021). Another hypothesis is that Num1 plays an active role in division, perhaps promoting or regulating Dnm1 function. Interestingly, a population of Dnm1 colocalizes with Num1 at the cell cortex (Cerveny *et al.*, 2007; Lackner *et al.*, 2013); however, the reason for this colocalization and the role of this population of Dnm1 remains unclear.

Here, we sought to further clarify the role of Num1 in mitochondrial division and address the relationship between Num1-mediated mitochondrial tethering and mitochondrial division. To this end, we developed a system to temporally control the formation and depletion of mitochondria-PM contact sites using regulatable versions of the native Num1 tether as well as an artificial tether. Using these tools, we found that mitochondrial division rates are reduced shortly after Num1-mediated mitochondrial tethering to the cell cortex is lost and are rescued shortly after tethering is induced. Surprisingly, using an artificial, Num1-independent-inducible tether, we found that mitochondria-PM tethering alone is not sufficient to rescue mitochondrial division and that a specific feature or function of Num1-mediated tethering is required. Tools for the temporal control of MCS formation and depletion using native and artificial membrane tethers, like those presented in this study, are useful to determine the distinct features and activities of MCS proteins that contribute to the biological functions of the MCS, as well as the kinetics of the events that occur downstream of MCS formation.

RESULTS

Loss of Num1 results in disrupted mitochondrial division

Num1 has been suggested to be required for mitochondrial division; cells lacking Num1 have been reported to have net-like mitochondrial networks and very few to no observable mitochondrial division events (Cerveny *et al.*, 2007; Hammermeister *et al.*, 2010). In contrast, our previous study suggests that Δ*dnm1* and Δ*num1* cells have distinct defects in mitochondrial morphology and, while mitochondrial division may be attenuated in the absence of Num1, Num1 does not play a direct role in mitochondrial division (Lackner *et al.*, 2013). To clarify the role of Num1 in mitochondrial division, we reexamined the morphology of mitochondria in wild-type, Δ*dnm1*, and Δ*num1* cells expressing mitochondrial-matrix-targeted dsRED (mito-Red) using high-resolution microscopy (Figure 1B). Mitochondrial morphology was analyzed on a per-cell basis and the networks were classified as follows: reticular (mitochondrial tubules interlaced yet spread apart, with few junctions), collapsed (mitochondrial tubules hard to distinguish from each other because they are entangled or clumped together), or netted (several closely apposed junctions in the mitochondrial network causing fenestrations; Figures 1C and Supplemental Figure S1). Cells lacking Num1 predominantly displayed a collapsed mitochondrial network, clearly distinct from the hyperfused, netted mitochondrial networks observed in the

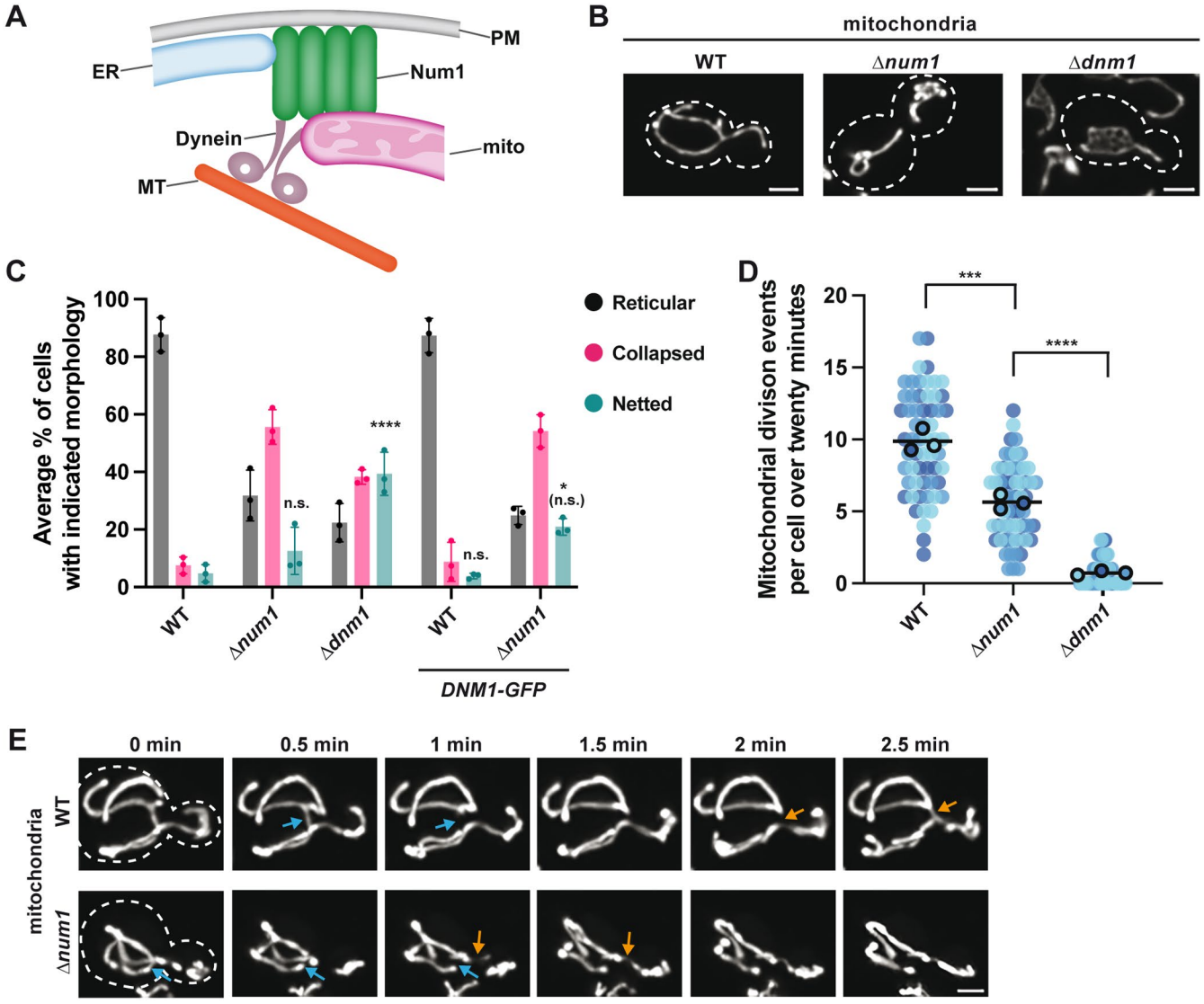

FIGURE 1: Num1 facilitates mitochondrial division. (A) Schematic of the MECA contact site. (B) Wild type (WT), Δ*num1*, and Δ*dnm1* cells expressing mito-Red were analyzed by fluorescence microscopy. Cells were grown in SCD at 30°C. Whole-cell maximum projections and single slice images are shown. The cell cortex is outlined with a white dashed line. Bar, 2 μm. (C) Quantification of mitochondrial morphology (either reticular, and collapsed, or netted) for WT, Δ*num1*, Δ*dnm1*, *DNM1-GFP* and Δ*num1 DNM1-GFP* cells is shown as the mean ± SD. Each black dot represents the average for one biological replicate, with >100 cells quantified per replicate. Three biological replicates are shown. Representative images of each morphology category are shown to the right. *p* values are in comparison to wild-type. * $p < 0.05$; **** $p < 0.0001$; ns, not significant (ordinary one-way ANOVA multiple comparisons). *p* values in parenthesis are in comparison to Δ*num1*. ns, not significant (unpaired *t* test). (D) Quantification of mitochondrial division events per cell in WT, Δ*num1*, and Δ*dnm1* cells expressing mito-Red over a 20-min time-lapse movie. Each dot represents a single cell. There are 20 cells per biological replicate, and the three biological replicates are represented in different colors. The black line denotes the grand mean. *p* values are in comparison to wild-type. *** $p < 0.001$, **** $p < 0.0001$ (ordinary one-way ANOVA multiple comparisons). (E) Examples of fusion and division events for WT and Δ*num1* cells expressing mito-Red are shown. Whole-cell maximum projections. Time-points are shown in min. Blue arrows indicate mitochondrial division events and orange arrows indicate mitochondrial fusion events. Bar, 2 μm.

majority of Δ*dnm1* cells (Figure 1, B and C). Through rigorous quantification of high-resolution time-lapse images, we observed that the number of division events over 20 min in Δ*num1* cells is lower than that observed in wild-type cells but greater than that observed in Δ*dnm1* cells (Figure 1, D and E). These results are consistent with our previous findings that mitochondria in Δ*num1* cells and Δ*dnm1* cells have distinct morphological defects and that mitochondrial division occurs at a reduced frequency in cells lacking Num1 (Lackner *et al.*, 2013).

We next sought to examine Dnm1-marked sites of mitochondrial division in Δ*num1* cells. We expressed Dnm1 as a yEGFP (GFP) fusion from its endogenous locus in Δ*num1* cells expressing mito-Red. Surprisingly, in comparison to Δ*num1* cells expressing untagged Dnm1, we observed an increase in the percentage of Δ*num1 DNM1-GFP* cells that display a hyperfused, netted mitochondrial network (12 and 21% of cells, respectively; Figure 1C). The netted phenotype was not as severe as a complete disruption of division, where 40% of Δ*dnm1* cells have a netted mitochondrial network (Figure 1C).

To further characterize the netted mitochondrial morphology, we quantified the severity of the phenotype using the number of fenestrations as a measure. For Δ*dnm1*, Δ*num1*, Δ*num1 DNM1-GFP, and DNM1-GFP* cells that were classified as having netted mitochondrial networks, we determined the percentage of these cells that had extensive netting (i.e., greater than three fenestrations in the mitochondrial net). We found that the percentage of Δ*num1* cells with extensive mitochondrial netting was lower than that observed for both Δ*dnm1* and Δ*num1 DNM1-GFP* cells (Supplemental Figure S2A). In our previous study, we did not observe netted mitochondrial networks in Δ*num1* cells expressing GFP-tagged Dnm1 (Lackner *et al.*, 2013). However, in that study, we expressed Dnm1-GFP from the plasmid pHS20, which was commonly used at the time to visualize Dnm1, in cells that also expressed untagged Dnm1 from the endogenous locus (Sesaki and Jensen, 1999). We replicated the results of our previous study, finding that a very small percentage of Δ*num1* cells (1.6% of cells) exhibited netted mitochondrial networks when Dnm1-GFP was expressed from a plasmid (Supplemental Figure S2B). These results indicate that the method used to visualize Dnm1 is likely the cause of the discrepant results and suggest that the increase in cells with netted mitochondrial networks is due to the expression of Dnm1-GFP from the endogenous locus. We hypothesize that the C-terminal GFP tag on Dnm1 partially compromises its function, creating a hypomorphic allele. In a wild-type background, the hypomorphic phenotype of Dnm1-GFP is not evident (Figure 1C). The phenotype only becomes apparent in the absence of Num1, when mitochondrial division is already compromised. The hypomorphic Dnm1 allele fortuitously provides us with a way to further enhance the mitochondrial division defect in Δ*num1* cells and more clearly assess the role of Num1 in mitochondrial division.

Characterizing a system to control the formation and depletion of mitochondria-ER-PM contact sites

To further assess the role of Num1 in mitochondrial division, we sought to develop a system in which we could control the formation and depletion of Num1-mediated contact sites. Such a system would allow us to ask whether and how quickly mitochondrial division could be restored following the induction of Num1-mediated mitochondrial tethering. We engineered an inducible Num1-mediated contact site using the rapamycin-inducible dimerization system. Because rapamycin inhibits the TOR pathway in yeast, we used a rapamycin-resistant strain background, which harbors the following mutations: Δ*fpr1 tor1-1* (Gruber *et al.*, 2006; Haruki *et al.*, 2008). We first confirmed that deletion of *NUM1* in the rapamycin-resistant background led to mitochondrial morphology and division defects similar to those observed in Δ*num1* cells (Supplemental Figures S2, C–E and Figure 1, B–D, respectively). Next, we appended the rapamycin-inducible dimerization components FRB-GFP and FKBP12 to Num1ΔPH (amino acids 1-2562) and the Num1 PH domain (Num1PH, amino acids 2563-2748), respectively (Figure 2A). Num1ΔPH-FRB-GFP was expressed from the endogenous *NUM1* locus and *FKBP12-NUM1PH* was integrated into the genome at the *URA3* locus and expressed from the TEF promoter. We refer to this strain as RID-Num1 for rapamycin-inducible dimerization of Num1. In the absence of rapamycin (uninduced RID-Num1 or uRID-Num1), Num1ΔPH-FRP-GFP was diffusely distributed throughout the cytosol (Figure 2B). Following the addition of rapamycin (induced RID-Num1 or iRID-Num1), cortical, mitochondria-associated clusters of Num1ΔPH-FRB-GFP were observed (Figure 2B and Supplemental Figure S3A, Video 1). We refer to these clusters as RID-Num1 clusters. We found that expression of FKBP12-Num1PH from the mid-strength TEF promoter best recapitulated wild-type Num1 cluster formation, mitochondrial tethering, and mitochondrial function when compared with expression from the comparatively weaker and stronger ADH and GPD promoters, respectively (Supplemental Figure S3, C and D). Formation of RID-Num1 clusters occurred rapidly following rapamycin addition; within 5 min the number of RID-Num1 clusters formed was comparable to the number of wild-type Num1 clusters (Figure 2, B and C). In addition, the mother-bud distribution of RID-Num1 clusters was similar to that of wild-type Num1 clusters; RID-Num1 clusters were observed predominantly in mother cells and large buds but were largely absent in small buds (Supplemental Figure S3B; Farkasovsky and Küntzel, 1995; Heil-Chapdelaine *et al.*, 2000). The RID-Num1 clusters also robustly tethered mitochondria to the PM (Figure 2D and Supplemental Figure S3A, Video 1). Thus, the RID-Num1 system provides a way to rapidly induce Num1-mediated mitochondria-PM tethering.

Next, we built upon the RID-Num1 system to make it reversible. We added an auxin-inducible degron (AID) tag to FKBP12-Num1PH, constructing FKBP12-AID-Num1PH, which we expressed in the rapamycin-resistant strain along with Num1ΔPH-FRB-GFP and Tir1. Tir1 is a plant specific F-box protein that binds the yeast SCF (Skp1, Cullin, F-box) complex. In the presence of auxin, Tir1 recruits the SCF complex to AID tagged proteins, which are subsequently ubiquitinated and targeted for proteasomal degradation (Nishimura *et al.*, 2009; Morawska and Ulrich, 2013). We refer to this modified RID-Num1 system as RID^{AID}-Num1 (Figure 3A). Similar to the RID-Num1 system, we observed RID^{AID}-Num1 clusters form at the PM following rapamycin addition in mother cells and large buds, and these clusters tethered mitochondria (Figure 3, B–D and Supplemental Figure S3B). The subsequent addition of auxin to induced RID^{AID}-Num1 (iRID^{AID}-Num1) cells resulted in the depletion of RID^{AID}-Num1 clusters (dRID^{AID}-Num1), with the maximal depletion occurring between 2 and 2.5 h after auxin treatment (Figure 3, B and C). Though this is longer than most AID-tagged protein depletions, it was not unexpected given that Num1 clusters are very stable and display limited exchange with the nonclustered pool of Num1 (Kraft and Lackner, 2017). Immunoblotting revealed that not only was FKBP12-AID-Num1PH degraded after auxin addition, but Num1ΔPH-FRB-GFP was also degraded, emphasizing the stability of Num1 clusters and strength of the rapamycin-induced dimerization interaction (Figure 3E, full blots in Supplemental Figure S4, A and B). As expected, in uninduced RID^{AID}-Num1 cells (uRID^{AID}-Num1), which were never exposed to rapamycin, the addition of auxin resulted in the degradation of FKBP12-AID-Num1PH, but not Num1ΔPH-FRB-GFP (Supplemental Figure S4C). Consistent with Num1 cluster depletion in dRID^{AID}-Num1 cells, mitochondria-PM tethering was also reduced in these cells, resulting in collapsed mitochondrial networks similar to those observed in Δ*num1* cells (Figure 3, B and D). Thus, by adding the AID tag to the RID-Num1 system, we have engineered a strain that allows us to induce and subsequently deplete Num1-mediated mitochondria-PM tethering and examine the downstream consequences.

Synthetic, regulatable Num1 contact sites behave like native Num1 contact sites

To fully validate the contact sites formed in the RID-Num1 and RID^{AID}-Num1 systems, it was important to establish that they function similarly to native Num1 contact sites, which have roles beyond mitochondria-PM tethering. Native Num1 clusters associate with the ER, in addition to mitochondria and the PM. We verified that RID-Num1 and RID^{AID}-Num1 clusters associate with the ER by live-cell microscopy. We examined the localization of RID-Num1 and RID^{AID}-Num1 clusters relative to the ER, and we found that 94%

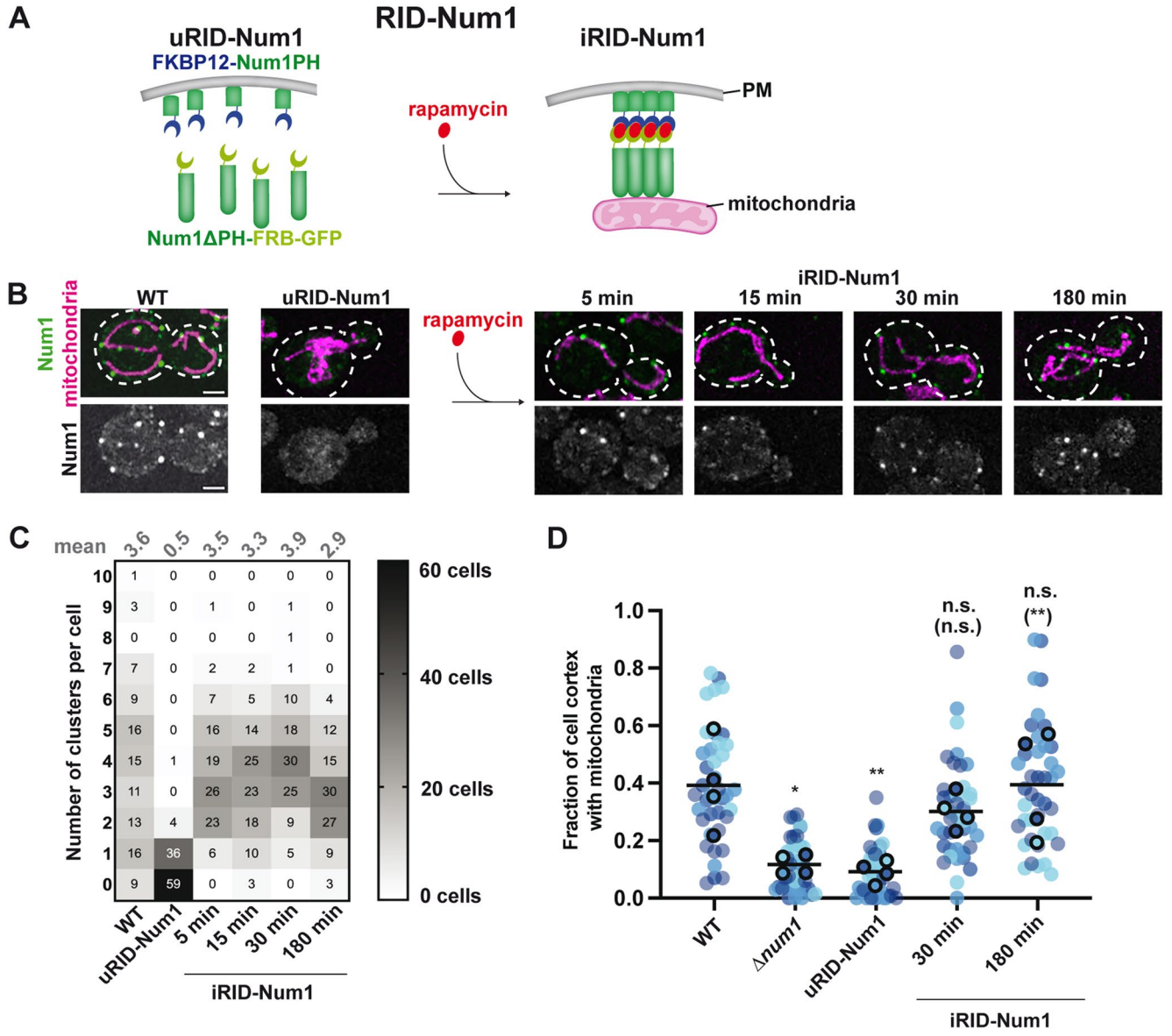

FIGURE 2: A regulatable system to control the formation of Num1 clusters. (A) Schematic depicting the rapamycin-induced dimerization (RID-Num1) system to inducibly form Num1-mediated contact sites. The left schematic represents the components of the uninduced RID-Num1 system before rapamycin addition, and the right schematic represents the RID-Num1 contact sites that form after dimerization is induced by rapamycin addition. uRID-Num1, uninduced RID-Num1; iRID-Num1, induced RID-Num1. (B) *NUM1-GFP* and RID-Num1 cells expressing mito-Red were analyzed by fluorescence microscopy. Whole-cell maximum projections are shown. The far left is a cell expressing *NUM1-GFP* and mito-Red with no rapamycin added. RID-Num1 cells are shown without (uRID-Num1) and with (iRID-Num1) rapamycin. A different cell is shown for each time-point. The top panel shows a merge of the GFP and mito-Red signals and the bottom panel shows the GFP signal in greyscale. Bar, 2 μm. (C) Quantification of the number of RID-Num1 clusters per cell for WT cells expressing *NUM1-GFP* and RID-Num1 cells. RID-Num1 cells were analyzed at the indicated times after rapamycin addition. $n = 100$ cells over three image replicates. (D) Quantification of the fraction of the cell cortex at mid-cell occupied by mitochondria for WT, Δ*num1*, uRID-Num1, and iRID-Num1 cells. Each dot represents a single cell and each biological replicate is represented by a different color. $n = 30$ cells. p values are in comparison to WT, p values in parenthesis are in comparison to uRID-Num1. * $p < 0.05$; ** $p < 0.01$; ns not significant (ordinary one-way ANOVA multiple comparisons).

of RID-Num1 clusters and 95% of RID^{AID}-Num1 clusters were colocalized with the ER, similar to the 94% of wild-type Num1 clusters that were colocalized with the ER (Figure 4, A and B). Because the cortical ER covers a significant portion of the cell cortex, we also examined the localization of RID-Num1 and RID^{AID}-Num1 clusters relative to the ER in Δ*lnp1* cells, in which the distribution of the cortical ER is disrupted, resulting in large ER-free regions at the cell cortex (Chen *et al.*, 2012). In the Δ*lnp1* background, the colocalization of RID-Num1 and RID^{AID}-Num1 clusters with ER was still apparent (95 and 96% respectively; Figure 4, A and B).

Additionally, we tested the ability of RID-Num1 and RID^{AID}-Num1 clusters to support mitochondrial and dynein function, which are both negatively affected by disruption of Num1 contact sites. In the absence of rapamycin, both uRID-Num1 and uRID^{AID}-Num1

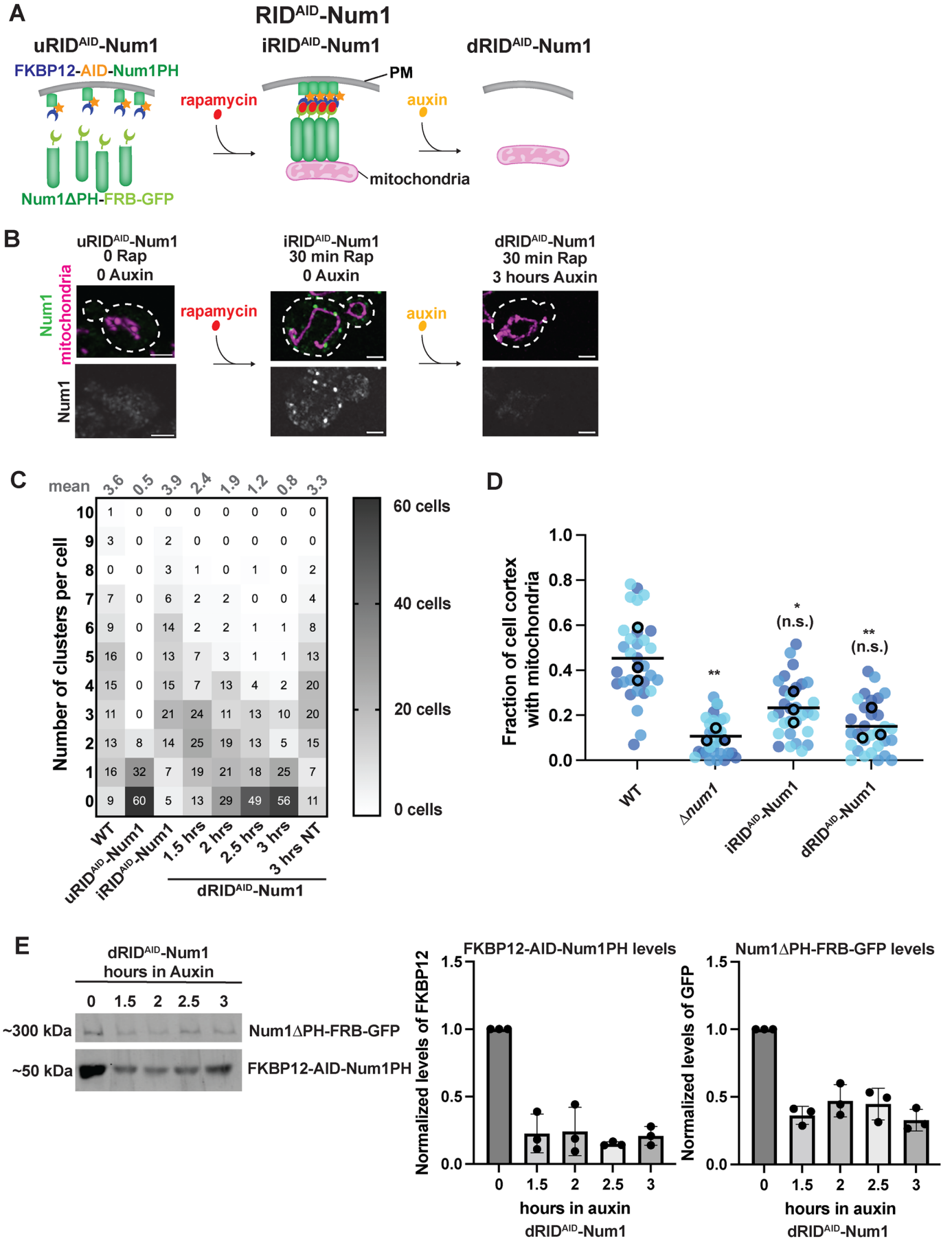
A
RIDAID-Num1
uRIDAID-Num1
iRIDAID-Num1
dRIDAID-Num1
FKBP12-AID-Num1PH
PM
rapamycin
auxin
mitochondria
Num1ΔPH-FRB-GFP
B
uRIDAID-Num1
0 Rap
0 Auxin
iRIDAID-Num1
30 min Rap
0 Auxin
dRIDAID-Num1
30 min Rap
3 hours Auxin
rapamycin
auxin
Num1
mitochondria
Num1
C
mean 3.6 0.5 3.9 2.4 1.9 1.2 0.8 3.3
Number of clusters per cell
60 cells
40 cells
20 cells
0 cells
WT
uRIDAID-Num1
iRIDAID-Num1
1.5 hrs
2 hrs
2.5 hrs
3 hrs
3 hrs NT
dRIDAID-Num1
D
Fraction of cell cortex with mitochondria
**
*
(n.s.)
**
(n.s.)
WT
Δnum1
iRIDAID-Num1
dRIDAID-Num1
E
dRIDAID-Num1
hours in Auxin
0 1.5 2 2.5 3
~300 kDa
Num1ΔPH-FRB-GFP
~50 kDa
FKBP12-AID-Num1PH
FKBP12-AID-Num1PH levels
Normalized levels of FKBP12
hours in auxin
dRIDAID-Num1
Num1ΔPH-FRB-GFP levels
Normalized levels of GFP
hours in auxin
dRIDAID-Num1

cells exhibited an impairment in respiratory growth, similar to that of Δ*num1* cells, as assessed quantitatively by colony size, indicative of a defect in mitochondrial function. In the presence of rapamycin, which induced RID-Num1 and RID^{AID}-Num1 cluster formation and restored mitochondrial tethering (Figures 2, A–D and 3, A–D), respiratory growth was rescued (Figure 4C). The subsequent addition of auxin to iRID^{AID}-Num1 cells resulted in a reduction in respiratory growth to a level similar to that observed for Δ*num1* cells, consistent with depletion of the RID^{AID}-Num1 clusters (Figure 4C).

Our previous study demonstrated that Num1-mediated cortical dynein anchoring is important for normal growth under respiratory conditions (White *et al.*, 2022). The increased respiratory growth observed for iRID-Num1 cells in comparison to the uninduced state suggests that RID-Num1 clusters are able to anchor dynein (Figure 4C). To further assess the ability of RID-Num1 clusters to anchor dynein as well as support dynein function in nuclear migration, we examined the growth of RID-Num1 cells in the absence of Kar9. Kar9 is required for a partially redundant nuclear inheritance pathway. Loss of both the dynein and Kar9 pathways for nuclear inheritance results in a severe growth defect (Miller and Rose, 1998). In a Δ*kar9* background, uRID-Num1 cells exhibited a severe growth defect, similar to Δ*kar9 NUM1ΔPH-FRB-GFP* cells (Figure 4, D and E). Following the addition of rapamycin, growth of the Δ*kar9* iRID-Num1 cells was significantly increased to near wild-type levels (Figure 4, D and E). These results indicate that RID-Num1 clusters support dynein function in nuclear inheritance. Finally, we found that there is a stable, cortical population of Dnm1 in iRID-Num1 cells (2.6 cortical Dnm1 foci per cell on average), equivalent to wild-type cells (Supplemental Figure S5, A and B, Video 2). Thus, the inducible and reversible synthetic Num1 tethers recapitulate the known activities of native Num1.

Tethering mitochondria to the PM with regulatable Num1 contact sites restores mitochondrial division

With the fully validated regulatable Num1 contact site systems in hand, we investigated the relationship between Num1 contact site formation/depletion and mitochondrial division. We first sought to determine whether we could restore mitochondrial division rates following the formation of Num1 contact sites. To this end, we quantified the number of mitochondrial division events in uRID-Num1 and iRID-Num1 over 20-min time-lapse movies. The uRID-Num1 strain had decreased mitochondrial division rates, comparable to Δ*num1* cells (Figure 5A). This indicates that mitochondrial division is impaired in the absence of mitochondria-ER-PM tethering, even when all domains of Num1 are present. 30 min after rapamycin addition, mitochondrial division rates in iRID-Num1 cells were increased in comparison to uRID-Num1 cells, and division rates remained consistently increased over uRID-Num1 at longer time points after rapamycin addition (Figure 5A). These results indicate that mitochondrial division rates are restored following the formation of Num1-mediated mitochondrial tethering sites.

We also examined mitochondrial morphology in RID-Num1 cells in the *DNM1-GFP* background, which exacerbates the division phenotype in cells lacking Num1. Because RID-Num1 also utilized GFP, we constructed a version that lacked GFP for these experiments. In uRID-Num1 *DNM1-GFP* cells, 35% of cells exhibited a collapsed mitochondrial network and 25% of cells exhibited a net phenotype, similar to Δ*num1 DNM1-GFP* cells (Figure 5B). In iRID-Num1 *DNM1-GFP* cells, near wild-type mitochondrial morphology was restored over time. 30 min after rapamycin addition, the percentage of iRID-Num1 cells with a collapsed mitochondrial network was dramatically reduced and the majority of cells exhibited a reticular mitochondrial network (Figure 5B). Interestingly, netted mitochondrial networks persisted (24% of cells) 30 min postrapamycin addition (Figure 5B). However, the percentage of iRID-Num1 cells with netted mitochondrial networks decreased to 19% 3 h after rapamycin addition, and further decreased to 12% 21 h after rapamycin addition (Figure 5B). These results suggest that mitochondrial morphology in cells with netted mitochondria takes longer to restore, perhaps because several mitochondrial division events are required to break apart the netted tubules. Eventually though, mitochondrial tethering with iRID-Num1 did rescue this division-related morphological defect.

We then used the RID^{AID}-Num1 system to measure the kinetics of disruption of mitochondrial division following the loss of mitochondria-PM contact. After 3 h in auxin, a timepoint where most dRID^{AID}-Num1 cells lacked Num1 clusters and cortical tethering of mitochondria was dramatically reduced (Figure 3, B–D), division rates dropped to levels comparable to uRID-Num1 and Δ*num1* cells (Figure 5C). These results indicate that when mitochondria-PM contact is lost, mitochondrial division is concurrently disrupted.

FIGURE 3: A regulatable system to deplete Num1 clusters. (A) Schematic depicting the rapamycin-induced dimerization auxin-inducible degradation (RID^{AID}-Num1) system to inducibly form and deplete Num1-mediated contact sites. The left schematic represents the components of RID^{AID}-Num1 before rapamycin addition, the middle schematic represents the Num1 contact sites that form after dimerization is induced by rapamycin addition, and the right schematic represents the system after addition of auxin and degradation of Num1 components. (B) RID^{AID}-Num1 cells expressing mito-Red were analyzed by fluorescence microscopy. Whole-cell maximum projections are shown. RID^{AID}-Num1 cells without any treatment (uRID^{AID}-Num1), with rapamycin added (iRID^{AID}-Num1), and with rapamycin and auxin added (dRID^{AID}-Num1) are shown. A different cell is shown for each condition. The top panel shows a merge of the GFP and mito-Red signals and the bottom panel shows the GFP signal in greyscale. Bar, 2 μm. (C) Quantification of the number of clusters per cell for WT cells expressing *NUM1-GFP* and RID^{AID}-Num1 cells. Data for WT are duplicated from Figure 2C. iRID^{AID}-Num1 cells were incubated with rapamycin for 30 min. dRID^{AID}-Num1 cells were incubated with rapamycin for 30 min, washed with media, and then incubated with auxin for the indicated times, in hours. The "3 h NT" sample was treated with rapamycin for 30 min, washed with media, and then incubated with no treatment for 3 h. n = 100 cells over three image replicates. (D) Quantification of the fraction of the cell cortex at mid-cell occupied by mitochondria for iRID^{AID}-Num1 and dRID^{AID}-Num1 cells. Data for WT and Δ*num1* are duplicated from Figure 2D. Each dot represents a single cell and each biological replicate is represented by a different color. n = 30 cells. p values are in comparison to WT, p values in parenthesis are in comparison to Δ*num1*. * $p < 0.05$; ** $p < 0.01$; ns not significant (ordinary one-way ANOVA multiple comparisons). (E) Western blot of RID^{AID}-Num1 components (detecting Num1ΔPH-FRB-GFP with an α-GFP antibody and FKBP12-Num1PH with an α-FKBP12 antibody). RID^{AID}-Num1 cells were incubated with rapamycin for 30 min, auxin was then added, and the cells were analyzed at the indicated times after auxin addition. Quantification of normalized protein levels is shown as the mean ± SD, n = 3 independent experiments. Total protein stain was used as a loading control (see Supplemental Figure S4B) as described in the *Materials and Methods*.

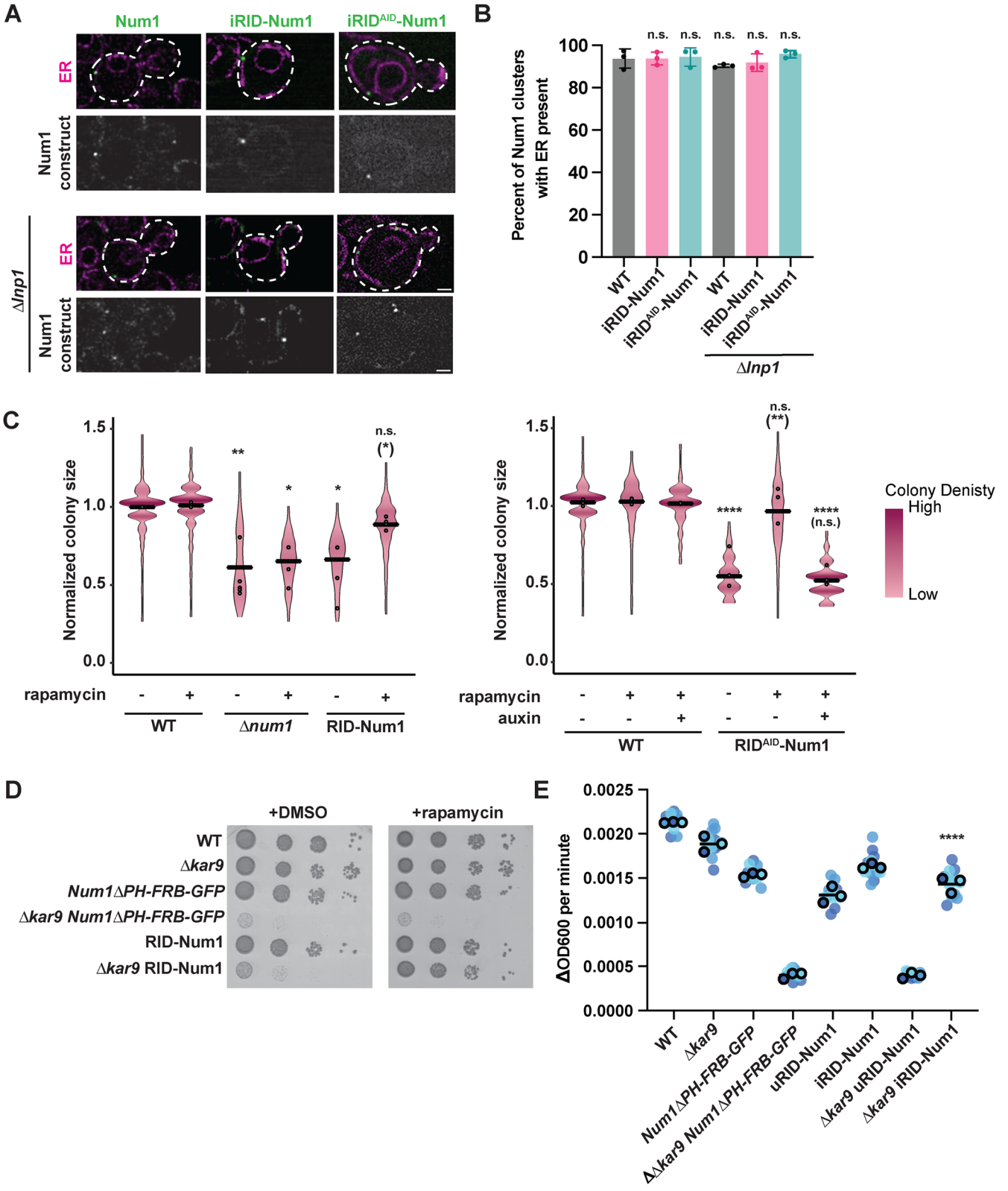

FIGURE 4: RID-Num1 and RID^{AID}-Num1 systems behave like wild-type Num1-mediated contact sites. (A) *NUM1-GFP*, RID-Num1, and RID^{AID}-Num1 cells expressing ER-Red in both WT and Δ*lnp1* backgrounds were analyzed by fluorescence microscopy. Single focal planes are shown. RID-Num1 and RID^{AID}-Num1 cells were imaged 30 min after rapamycin addition. Bar, 2 μm. (B) Quantification of the percent of Num1 clusters with ER present per cell for WT, RID-Num1, and RID^{AID}-Num1 cells in both WT and Δ*lnp1* backgrounds is shown as the mean ± SD. RID-Num1 and RID^{AID}-Num1 cells were imaged 30 min after rapamycin addition. Each dot represents the average for one biological replicate, with >10 cells and >20 clusters per replicate. Three biological replicates are shown. *p* values are in comparison to WT. ns not significant (Kruskal-Wallis test multiple comparisons). (C) Quantification of WT, Δ*num1*, RID-Num1, and RID^{AID}-Num1 colony size, with cells grown at 35°C in respiratory growth conditions (YPEG solid media) for 5 d. DMSO

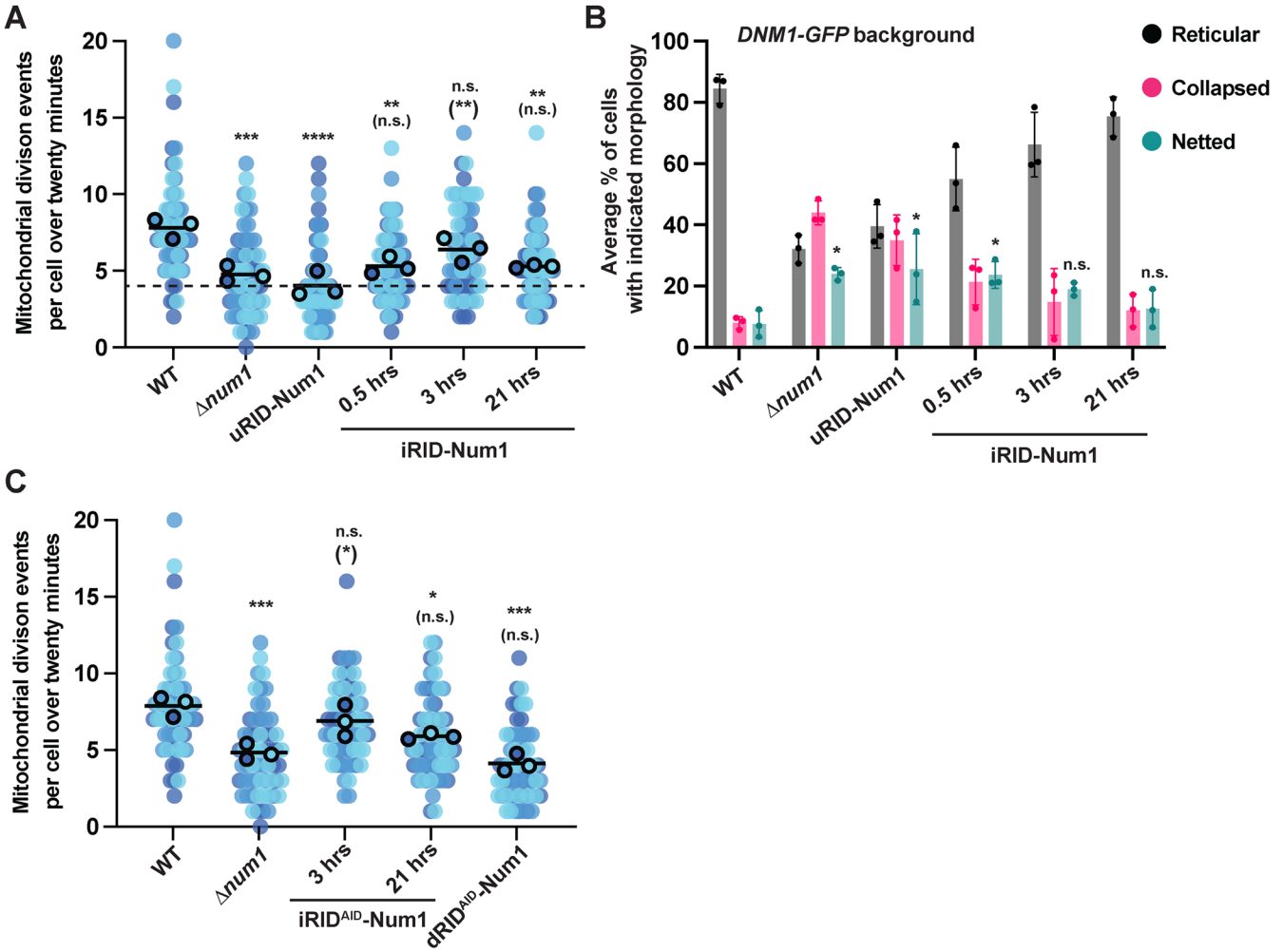

FIGURE 5: The RID-Num1 and RID^{AID}-Num1 systems provide insight into the connection between Num1-mediated contact sites and mitochondrial division. (A) Quantification of mitochondrial division events per cell over a 20-min time-lapse movie for RID-Num1 cells treated with rapamycin for the indicated times. Each dot represents a single cell. There are 20 cells per biological replicate, and the three biological replicates are represented in different colors. The black line denotes the grand mean. *p* values are in comparison to WT, *p* values in parenthesis are in comparison to uRID-Num1. ** $p < 0.01$; *** $p < 0.001$; **** $p < 0.0001$; ns not significant (ordinary one-way ANOVA multiple comparisons). (B) Quantification of mitochondrial morphology (either reticular and collapsed, or netted) for RID-Num1 cells is shown as the mean ± SD. Time-points after addition of rapamycin are shown. Data for WT and Δ*num1* are duplicated from Figure 1C. Each dot represents the average for one biological replicate, with >100 cells per replicate. Three biological replicates are shown. *p* values are in comparison to WT. * $p < 0.05$; ns not significant (ordinary one-way ANOVA multiple comparisons). (C) Quantification of mitochondrial division events per cell over a 20-min time-lapse movie for RID^{AID}-Num1 cells. iRID^{AID}-Num1 cells were incubated with rapamycin for the indicated times. dRID^{AID}-Num1 cells were incubated with rapamycin for 21 h and then auxin was added for 3 h before imaging. Each dot represents a single cell. There are 20 cells per biological replicate, and the three biological replicates are represented in different colors, with the average value outlined in black. The black line denotes the grand mean. *p* values are in comparison to WT, *p* values in parenthesis are in comparison to Δ*num1*. * $p < 0.05$; *** $p < 0.001$; ns not significant (ordinary one-way ANOVA multiple comparisons).

(1 μM), rapamycin (1 μM), or auxin (1 mM) was added to plates, as indicated. The graph is a violin plot of the radius (in pixels) of colonies normalized to the mean radius of WT colonies for the respective experiment. The black line denotes the grand mean of at least three independent experiments and dots depict the mean of each experiment. $n > 300$ colonies. *p* values are in comparison to WT, *p* values in parenthesis are in comparison to RID-Num1 without rapamycin and RID^{AID}-Num1 without rapamycin or auxin, respectively. * $p < 0.05$; ** $p < 0.01$; **** $p < 0.0001$; ns not significant (Kruskal-Wallis test multiple comparisons). (D) Spot-test growth assay of WT, Δ*kar9*, *NUM1ΔPH-FRB-GFP*, Δ*kar9 NUM1ΔPH-FRB-GFP*, RID-Num1, and Δ*kar9* RID-Num1 strains in fermentative growth conditions (YPD solid media) at 30°C for 1 d. DMSO or 1 μM rapamycin were added to plates, as indicated. (E) The change in OD_{600} per min for the linear portion of the growth curves obtained using a microplate reader for WT, Δ*kar9*, *NUM1ΔPH-FRB-GFP*, Δ*kar9 NUM1ΔPH-FRB-GFP*, RID-Num1, and Δ*kar9* RID-Num1 strains in fermentative growth conditions (YPD media) at 30°C for 1 d. Dots represent biological replicates, each composed of three to four technical replicates; mean ± SD is shown. *p* values are in comparison to Δ*kar9* uRID-Num1. **** $p < 0.0001$ (ordinary one-way ANOVA multiple comparisons).

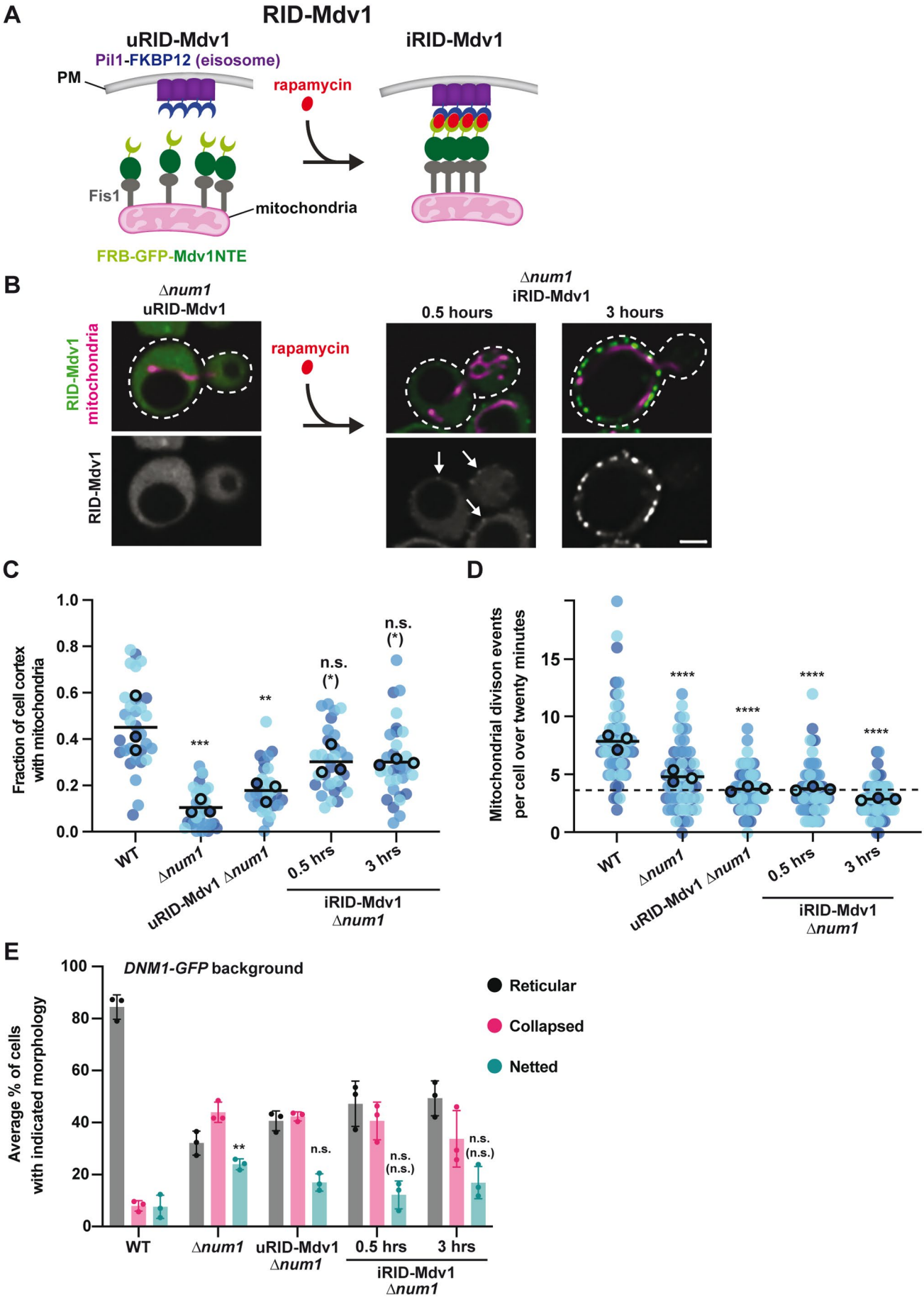
A
RID-Mdv1
uRID-Mdv1
iRID-Mdv1
Pil1-FKBP12 (eisosome)
PM
rapamycin
Fis1
mitochondria
FRB-GFP-Mdv1NTE
B
Δnum1
uRID-Mdv1
Δnum1
iRID-Mdv1
0.5 hours
3 hours
rapamycin
RID-Mdv1
mitochondria
RID-Mdv1
C
Fraction of cell cortex with mitochondria
1.0
0.8
0.6
0.4
0.2
0.0
***
**
n.s. (*)
n.s. (*)
WT
Δnum1
uRID-Mdv1 Δnum1
0.5 hrs
3 hrs
iRID-Mdv1 Δnum1
D
Mitochondrial divison events per cell over twenty minutes
15
10
5
0
****
****
****
****
WT
Δnum1
uRID-Mdv1 Δnum1
0.5 hrs
3 hrs
iRID-Mdv1 Δnum1
E
DNM1-GFP background
Average % of cells with indicated morphology
100
80
60
40
20
0
Reticular
Collapsed
Netted
**
n.s.
n.s. (n.s.)
n.s. (n.s.)
WT
Δnum1
uRID-Mdv1 Δnum1
0.5 hrs
3 hrs
iRID-Mdv1 Δnum1

Num1-mediated mitochondria-plasma membrane tethering is favorable for mitochondrial division

The data presented above indicate that mitochondrial division rates are restored following the formation of Num1-mediated mitochondria-tethering sites. However, based on these data, we cannot discern whether the role of Num1 in mitochondrial division extends beyond tethering mitochondria to the PM. To test whether simply tethering mitochondria to the PM is sufficient to increase rates of mitochondrial division, we engineered an inducible mitochondria-PM tethering system that is independent of Num1. In this system, we expressed the mitochondria-binding domain of Mdv1 (amino acids 1-241, which is also known as the Mdv1 N-terminal extension; Mdv1NTE), as a fusion to FRB-GFP (Figure 6A; Tieu *et al.*, 2002; Cerveny and Jensen, 2003; Zhang and Chan, 2007). FRB-GFP-Mdv1NTE was expressed from an exogenous locus so the native *MDV1* gene was not disrupted. Because Mdv1 is involved in mitochondrial division, we verified that the expression of FRB-GFP-Mdv1NTE in an otherwise wild-type background did not affect mitochondrial division. Mitochondrial division rates in wild-type cells expressing FRB-GFP-Mdv1NTE were similar to those in wild-type cells that did not express FRB-GFP-Mdv1NTE (Supplemental Figure S6A). This result is consistent with a previous study in which expression of Mdv1NTE in wild-type cells did not have a negative effect on mitochondrial division (Tieu *et al.*, 2002). To recruit FRB-GFP-Mdv1NTE to the PM in the presence of rapamycin, we co-expressed Pil1 as a fusion to the other component of the rapamycin-induced dimerization system, FKBP12 (Figure 6A). Pil1 is a major component of eisosomes, which are multi-protein assemblies that form discrete, stable puncta at the PM (Walther *et al.*, 2006). We refer to this artificial mitochondria-PM tether as RID-Mdv1 (Figure 6A). RID-Mdv1 is an inducible version of a constitutive Mdv1NTE-Pil1 artificial tether we used previously to test whether restoring contact or proximity between mitochondria and the PM was able to rescue the respiratory growth defect of Δ*num1* cells (White *et al.*, 2022).

We examined whether RID-Mdv1-mediated mitochondria-PM tethering was able to rescue mitochondrial morphology and division rates in cells lacking Num1 (Figure 6, B–D). In RID-Mdv1 Δ*num1* cells in the absence of rapamycin (uRID-Mdv1), FRB-GFP-Mdv1 was localized diffusely in the cytosol and the mitochondrial division defect observed was similar to that observed in Δ*num1* cells (Figure 6, B and D). Following the addition of rapamycin, induced RID-Mdv1 (iRID-Mdv1) clusters on the PM were visible within 30 min and became more abundant after 3 h (Figure 6B). Consistent with the formation of cortical RID-Mdv1 clusters, cortical mitochondrial tethering was restored to iRID-Num1 and iRID^{AID}-Num1 levels in iRID-Mdv1 Δ*num1* cells 30 min after rapamycin addition (Figures 2D, 3D, and 6C). We then assessed division rates in iRID-Mdv1 Δ*num1* cells. In contrast to the increase in division rates observed in iRID-Num1 and iRID^{AID}-Num1 cells compared with the uninduced state (Figure 5, A and C), there was no increase in mitochondrial division rates in iRID-Mdv1 Δ*num1* cells (Figure 6D), despite the fact that cortical tethering of mitochondria was restored to similar extents in iRID-Mdv1, iRID-Num1 and iRID^{AID}-Num1 cells (Figures 6C, 2D, and 3D). As a control for using eisosomes as the PM-anchoring component of the RID-Mdv1 tether, we also targeted NUM1ΔPH-FRB-GFP to eisosomes using Pil1-FKBP12. We have previously used a constitutive version of this mitochondria-PM tether that we refer to as PAN, for Pil1-associated Num1 (Schmit *et al.*, 2018). Therefore, we named the inducible version of the tether RID-PAN. In comparison to uRID-PAN cells, which exhibited division rates similar to Δ*num1* cells, division rates were increased in iRID-PAN cells, similar to iRID-Num1 cells (Supplemental Figure S6B and Figure 5A, respectively). Thus, the PM targeting component does not determine the ability of the tethers to rescue mitochondrial division.

We also examined mitochondrial morphology in uRID-Mdv1 and iRID-Mdv1 Δ*num1* cells in the *DNM1-GFP* background, which exacerbates the mitochondrial division defect in cells lacking Num1. We found that the percentage of cells that exhibited netted mitochondrial networks did not change following the formation of RID-Mdv1 tethers (Figure 6E), consistent with our finding that division rates were not rescued following RID-Mdv1-mediated mitochondrial-PM tethering (Figure 6D). In addition, few to no stable cortical Dnm1 foci were observed in RID-Mdv1 cells (Supplemental Figure S5B), which is consistent with previous studies that suggest that mitochondria-PM tethering alone is not sufficient to establish the stable, cortical population of Dnm1 (Schauss *et al.*, 2006; Lackner *et al.*, 2013). Together, these results indicate that restoring mitochondria-PM contact with the RID-Mdv1 tether is not sufficient to rescue the mitochondrial division defect observed in the absence of Num1.

FIGURE 6: Num1-independent mitochondrial-PM tethering is not favorable for mitochondrial division. (A) Schematic depicting the Num1-independent rapamycin-induced dimerization system using the NTE domain of Mdv1 (RID-Mdv1). The schematic on the left shows the FRB-GFP-Mdv1 and Pil1-FKBP12 constructs before addition of rapamycin and the panel on the right shows the assembled mitochondria-PM tether after rapamycin addition. (B) RID-Mdv1 cells expressing mito-Red were analyzed by fluorescence microscopy. Single mid-slice images are shown. RID-Mdv1 cells without any treatment (uRID-Mdv1) and with rapamycin added (iRID-Mdv1) are shown. A different cell is shown for each condition. The top panel shows a merge of the GFP and mito-Red signals and the bottom panel shows the GFP signal in greyscale, with consistent brightness/contrast. White arrows indicate RID-Mdv1 clusters for iRID-Mdv1 after 30 min of rapamycin addition. Bar, 2 μm. (C) Quantification of the fraction of the cell cortex at mid-cell occupied by mitochondria for RID-Mdv1 cells. Data for WT and Δ*num1* are duplicated from Figure 2D. Each dot represents a single cell, and each biological replicate is represented by a different color. $n = 30$ cells. p values are in comparison to WT, p values in parenthesis are in comparison to uRID-Mdv1 Δ*num1*. * $p < 0.05$; ** $p < 0.01$; *** $p < 0.001$; ns not significant (ordinary one-way ANOVA multiple comparisons). (D) Quantification of mitochondrial division events per cell over a 20-min time-lapse movie for RID-Mdv1 cells treated with rapamycin for the indicated times. Data for WT and Δ*num1* are duplicated from Figure 5A. Each dot represents a single cell. There are 20 cells per biological replicate, and the three biological replicates are represented in different colors. The black line denotes the grand mean. p values are in comparison to WT. **** $p < 0.0001$ (ordinary one-way ANOVA multiple comparisons). (E) Quantification of mitochondrial morphology (either reticular and collapsed, or netted) for RID-Mdv1 cells expressing Dnm1-GFP is shown as the mean ± SD. Time-points after addition of rapamycin are shown. Data for WT and Δ*num1* are duplicated from Figure 5B. Each dot represents the average for one biological replicate, with >100 cells per replicate. Three biological replicates are shown. p values are in comparison to WT, p values in parenthesis are in comparison to uRID-Mdv1 Δ*num1*. ** $p < 0.01$; ns not significant (ordinary one-way ANOVA multiple comparisons).

Using the artificial tethering system, we next investigated whether the function of Num1 in mitochondrial division could be separated from its role as a cortical tether. To this end, we expressed Num1ΔPH-GFP in cells in which mitochondria were artificially tethered to the cell cortex using RID-Mdv1. We found that the expression of Num1ΔPH-GFP did not increase rates of mitochondrial division in RID-Mdv1 cells (Supplemental Figure S6C). These results indicate that the function of Num1 in mitochondrial division requires the association of Num1 with the PM, even when cortical tethering of mitochondria is restored via artificial means. In total, our findings suggest that a specific feature of Num1-mediated mitochondrial tethering positively impacts mitochondrial division.

DISCUSSION

One of the many functions ascribed to Num1 is a role in mitochondrial division (Cerveny *et al.*, 2007). Here, we rigorously dissect this role and clarify that Num1 is not required for mitochondrial division, consistent with our previous study (Lackner *et al.*, 2013), but does enhance mitochondrial division. To investigate the relationship between Num1-mediated mitochondrial tethering and mitochondrial division, we designed a novel, regulatable version of the native Num1 tether, called RID-Num1. While regulatable artificial membrane tethers have been used to study MCS functions (Csordás *et al.*, 2010; Booth *et al.*, 2016, 2021; Kwak *et al.*, 2020; Benedetti, 2021; Katona *et al.*, 2022; Amado *et al.*, 2023), this is the first use of an inducible dimerization system to reconstitute a native MCS. By combining the rapamycin-inducible dimerization system with the auxin-inducible degradation system, we developed a system called RID^{AID}-Num1, in which we were able to establish and deplete native Num1-mediated mitochondrial tethering sites. We found that depletion of Num1-mediated contact sites results in a concurrent reduction of mitochondrial division rates, and that mitochondrial division rates are increased shortly after the reestablishment of Num1-mediated mitochondrial tethering. Furthermore, the increase in mitochondrial division rates following the induced formation of RID-PAN tethers, in which eisosomes are used in place of the Num1 PH domain as the PM-anchoring component, indicates that the PH domain does not play a role in mitochondrial division beyond targeting Num1 to the PM. Together, these results support the idea that Num1-mediated tethering facilitates mitochondrial division.

To determine whether the role of Num1 in mitochondrial division extends beyond simply tethering mitochondria to the PM, we developed a regulatable tethering system, RID-Mdv1, to increase mitochondria-PM contact in a Num1-independent manner. We found that even though RID-Mdv1 restored cortical mitochondria tethering in the absence of Num1, mitochondrial division rates were not restored. Artificial Num1-independent tethers have been used previously to examine the function of Num1 in mitochondrial division (Klecker *et al.*, 2013). These tethers were found to partially restore wild type-like mitochondrial morphology in Δ*num1* cells, similar to what we observed for the iRID-Mdv1 tether, which rescued the cortical tethering of mitochondria in Δ*num1* cells. While we use mitochondrial division rates as a metric to examine the effect of iRID-Mdv1-mediated tethering on mitochondrial division in Δ*num1* cells, Klecker *et al.* 2013 use azide-induced mitochondrial fragmentation as a metric and observe mitochondrial fragmentation in only ~30% of Δ*num1* cells expressing the artificial tethers after azide treatment. Therefore, while our study and Klecker *et al.* 2013 demonstrate that artificial tethers can rescue the cortical distribution of mitochondria in the absence of Num1, the effects of the tethers on mitochondrial division cannot be directly compared. In our study, we examine mitochondrial division rates, not azide-induced fragmentation, and observe that iRID-Mdv1-mediated tethering has no effect on the rates of mitochondrial division in Δ*num1* cells. Thus, our findings suggest there is a specific feature of Num1-mediated mitochondrial tethering that facilitates mitochondrial division.

One possible explanation for these results is that Num1-mediated tethering exerts an ideal amount of tension across the mitochondrial membrane for mitochondrial division to occur. Several studies have found a connection between mitochondrial membrane tension and membrane division (Roux *et al.*, 2006; Mahecic *et al.*, 2021). There are, on average, 3–4 Num1-mediated mitochondrial tethering sites per cell that are spaced out along the cell cortex (Figure 2, B and C; Kraft and Lackner, 2017). It is possible that the placement and number of Num1 clusters creates an ideal tethering geometry to facilitate mitochondrial division. While RID-Mdv1 increases mitochondria-PM contact, the number and placement of the tethering sites differ from Num1 tethering sites, which may explain why mitochondrial division rates were not restored in the iRID-Mdv1 cells. However, the finding that division rates were partially restored in iRID-PAN cells argues against this possibility as the number and placement of tethering sites in iRID-PAN and iRID-Mdv1 cells should be similar.

A second possibility is that a lack of ER tethering at RID-Mdv1 mitochondria-PM tethering sites could explain the inability of RID-Mdv1 to rescue the division defect observed in Δ*num1* cells. Unfortunately, attempts to introduce ER-tethering motifs/domains to the RID-Mdv1 tether were not successful. Therefore, we are not able to rule out the possibility that the presence of the ER at mitochondria-PM tethering sites positively impacts mitochondrial division. We are very interested in the association of Num1 with the ER and are actively pursuing experiments to characterize the Num1-ER association and its functions.

Finally, it is possible that fully reconstituted Num1 regulates mitochondrial division factors, such as Dnm1. It is clear from experiments comparing uRID-Num1 and iRID-Num1 as well as experiments in which Num1ΔPH is expressed in the presence of the artificial tethering system that fully reconstituted Num1 has a positive impact on mitochondrial division. There is a population of Dnm1 that colocalizes with cortical Num1 clusters overtime (Cerveny *et al.*, 2007; Lackner *et al.*, 2013), and this population is present in RID-Num1, but not RID-Mdv1, cells. While this population of Dnm1 does not appear to be actively participating in mitochondrial division (Lackner *et al.*, 2013), there is likely a functional purpose for the colocalization of Dnm1 with Num1 clusters. It is possible that Num1 could be recruiting and holding Dnm1 in close proximity to the mitochondrial membrane, acting like a reservoir for Dnm1 so it is accessible when needed. Alternatively, Dnm1 may be playing a division-independent role at this tripartite membrane contact site.

The regulatable MCS systems engineered for this study have broad applications for studying MCS biology and the spatial and temporal relationship between the formation of a MCS and the functions attributed to that MCS. Historically, deletions or mutations of contact site proteins have been used to study MCS functions. Regulatable contact sites are advantageous to these nonconditional mutants; they provide the ability to deplete and reestablish MCSs and observe the downstream consequences in real time, which proved valuable in examining the relationship between Num1-mediated mitochondrial tethering and mitochondrial division. The utility of the regulatable native and artificial tethers described here extends beyond this study. We have employed RID-Num1 and RID-Mdv1 to assess a novel connection between MECA and the distribution of lipid species in the PM (manuscript in prep). Also, it is

likely possible to expand the use of RID-Num1 and RID^{AID}-Num1 to other eukaryotic cells. Because Num1 recognizes conserved features of the mitochondrial membrane and PM (Yu *et al.*, 2004; Ping *et al.*, 2016; Kraft and Lackner, 2019), it is possible that the regulatable Num1 tether can be used as an exogenous system in other eukaryotic cells to control mitochondrial positioning relative to the PM. Given the rapidly growing field of MCS biology and the functional complexity of the proteins that form MCSs, tools such as those described here will be critical for diving deeper into the mechanisms underlying the cellular processes facilitated by MCSs.

MATERIALS AND METHODS

Request a protocol through *Bio-protocol*.

Strains and plasmids

Supplemental Tables 1 and 2 list all strains and primers used for this study, respectively. Strains were constructed using standard yeast techniques (PCR-based targeted homologous recombination and transformation). Primer sets used to amplify deletion cassettes are named F1 and R1 and primer sets used to amplify C-terminal gene tagging cassettes are named F5 and R3 (Longtine *et al.*, 1998; Janke *et al.*, 2004; Sheff and Thorn, 2004). Plasmids used in this study are listed in Supplemental Table 3. For imaging mitochondria, strains were transformed with EcoRI digested pLL19 (pRS305 *mito-dsRed::LEU/NAT*; Abrish *et al.*, 2020). All strains and plasmids will be made available upon request.

Imaging

For Figures 1B, C, and E, 3B, C, and D, 5B, 6B, C, and E, Supplemental Figures S1, S2A, B, D, and E, S3A–C, and S5A–B, all strains were grown to mid-log phase in synthetic complete +2% (wt/vol) dextrose media with 2x adenine (SCD). A final concentration of 1 μM rapamycin was added to cells notated as iRID-Num1, iRID^{AID}-Num1, or iRID-Mdv1 and incubated for the indicated time before imaging. For dRID^{AID}-Num1 cultures, 1 μM rapamycin was added for 30 min, and then 1 mM auxin at pH 6.4 was added for the indicated time before imaging. Cells were imaged on an agarose pad on a depression slide. Single time-point images were captured on a Nikon Spinning Disk Confocal System fitted with a CSU-W1 dual-disk spinning disk unit (Yokogawa). A 60X (NA-1.42) objective and a Hamamatsu ORCA Fusion Digital CMOS camera were used for image capture. Images were captured and deconvolved with Elements software (Nikon).

For Figures 1D, Supplemental Figures S2D, and S6A–B all strains were grown to mid-log phase in synthetic complete +2% (wt/vol) dextrose media with 2x adenine (SCD). Cells were imaged on concanavalin A-treated dishes (2 mg/ml in water). 20-min time-lapse movies with 30 s time-points were captured on a Nikon Spinning Disk Confocal System (described above).

For Figure 2B–D, all strains were grown to mid-log phase in synthetic complete +2% (wt/vol) dextrose media with 2x adenine (SCD). A final concentration of 1 μM rapamycin was added to some of the cultures for various lengths of time, as indicated in the figure. Cells were imaged on an agarose pad on a depression slide. Single time-point images were captured on a Leica Spinning Disk Confocal System fitted with a CSU-X1 spinning-disk head (Yokogawa). A PLAN APO 100X (NA-1.44) and an Evolve 512 Delta EMCCD camera (Photometrics) were used for image capture. Images were captured with Metamorph (Molecular Devices) and deconvolved using AutoQuant X3's (Media Cybernetics) iterative, constrained, three-dimensional deconvolution method. Linear adjustments to brightness and contrast were performed using FIJI and Photoshop (Adobe). Deconvolved images are shown in the figure.

For Figure 4A–B, all strains were grown to mid-log phase in synthetic complete +2% (wt/vol) dextrose media with 2x adenine (SCD). Cells were imaged on an agarose pad on a depression slide. Single time-point images were captured on a Leica TCS SP8 LSCM. A 63X (NA-1.4) objective and HyD detectors were used for image capture. Huygens software was used for image deconvolution.

For Figures 5, A and C, and 6D all strains were grown to mid-log phase in synthetic complete +2% (wt/vol) dextrose media with 2x adenine (SCD). A final concentration of 1 μM rapamycin was added to cells notated as iRID-Num1, iRID^{AID}-Num1, and iRID-Mdv1 and incubated for the indicated times before imaging. For dRID^{AID}-Num1 cultures, 1 μM rapamycin was added for 21 h, and then 1 mM auxin at pH 6.4 was added for 3 h before imaging. Cells were imaged on concanavalin A-treated dishes (2 mg/ml in water). 20-min time-lapse movies with 30 s time-points were captured on a Nikon Spinning Disk Confocal System (described above).

Image Quantifications

For mitochondria morphology quantifications, single time-point maximum projection images were analyzed on a per cell basis; each cell's mitochondrial network was classified as reticular, collapsed, or netted. See Supplemental Figure S1 for examples of each phenotype. For each strain in Supplemental Figure S2A, the population of cells with netted mitochondria was analyzed for number of fenestrations by manually counting the fenestrations per cell.

For mitochondrial division event quantifications, a 20-min time-lapse maximum projection movie with 30 s time-points was analyzed and events of mitochondrial division were counted on a per cell basis.

For Num1-GFP, RID-Num1, and RID^{AID}-Num1 cluster quantifications, single time-point maximum projection images were analyzed for the number of GFP foci.

For mitochondria-plasma membrane contact quantifications, the proportion of the cell cortex in which mitochondrial signal was present was quantified similar to Kraft and Lackner (Kraft and Lackner, 2019). A 5-pixel wide line was drawn around the circumference of the cell in FIJI software. The intensity values of the mitochondria channel were collected along the drawn line. Background intensity values were determined by drawing a 5 μm long, 5-pixel wide line in the background for each field of view used. The number of data points above the average background intensity value for the corresponding field of view divided by the total number of data points was plotted.

For Num1-GFP, RID-Num1, and RID^{AID}-Num1 cluster ER association quantifications, single time-point, single slice images were used to score if a GFP foci overlapped with ER signal.

To quantify the percent of cells with Num1-GFP, RID-Num1, and RID-Mdv1 clusters present in the bud, single time-point, maximum projection images were analyzed for the number of GFP foci in the bud. Small and large buds were classified as having a bud: mother diameter of less than or greater than 1:3, respectively, as measured in FIJI.

To quantify the number of cortical Dnm1-GFP foci per cell, a 2-min time-lapse maximum projection movie with 30 s time-points was analyzed for Dnm1-GFP foci that persisted for the entire movie.

Western blots

Cells were grown to mid-log in yeast extract/peptone with 2% (wt/vol) dextrose (YPD), with 1 μM rapamycin and/or 1 mM auxin added for the time indicated in the figure. Cells were harvested by centrifugation (3000 × g for 1 min) and whole-cell extracts were prepared by a NaOH lysis and trichloroacetic acid precipitation procedure.

Pellets were resuspended in 50 µl of MURB (100 mM MES, pH 7, 1% SDS, and 3 M urea). Whole-cell extracts were analyzed by SDS–PAGE and Western Blot using Revert Total Protein Stain (LI-COR Biosciences) as a control. Antibodies used were anti-GFP (Abclonal Rabbit anti-GFP-Tag pAb 1:2000) and anti-FKBP12 (Abcam Rabbit anti-FKBP12 ab2918 1:1000) as primaries and goat antirabbit IgG DyLight 800 (Thermo Fisher Scientific 1:15,000) as a secondary antibody. The total protein stain and immunoreactive bands were detected with the Odyssey Infrared Imaging System (LI-COR Biosciences). Western blots were quantified using ImageStudio (LI-COR Biosciences) by normalizing the intensity of the immunoreactive band of interest to the total protein for each sample.

Growth assays

To analyze growth by serial dilution, cells were grown in YPD medium overnight at 30°C. Cells were diluted and allowed to grow to mid-log at 30°C, then 0.2 OD_{600} of cells were pelleted (3000 × g for 1 min) and resuspended in water to a final OD_{600} of 0.5. Five-fold serial dilutions were conducted, spotted onto YPD or YPEG agar plates, and grown at 37°C as indicated.

To analyze growth quantitatively by colony size, cells were grown as described above to achieve mid-log growth. Analysis was performed as described in White *et al.* (White *et al.*, 2022). Two 1:100 serial dilutions were performed to achieve cell concentrations of ~1000 cells/ml. 150 µl of the diluted-cell culture were plated onto both YPD and YPEG plates to achieve roughly 100–150 individual colonies per plate and left to grow at 35°C. YPD plates were removed from the incubator after 48 h of growth, and YPEG plates were removed from the incubator after 120 h of growth. For analysis, plates were scanned and images were analyzed using OpenCFU software to identify the radius (in pixels) of individual colonies as a measure of colony size (Geissmann, 2013). In the analysis, colonies were excluded if: 1) the box that defined the area measured for a particular colony encompassed more than one colony; 2) the box that defined the area measured did not completely encompass the colony being measured; or 3) if colony morphology was significantly impacted by touching the side of the plate or other colonies, such that area being measured was not accurate. All strains were normalized to the average colony size of the wild-type sample grown in the same condition on the same day. Specifically, for each round of the assay, the average radius size of wild-type colonies was determined for each condition. Colony size for all of the strains from the same experimental round and condition was divided by the average radius size of wild-type colonies. For graphs that include data collated from experiments that were each normalized to their own wild-type data set, the wild-type data sets from all experiments are included in the graph. In addition to showing the grand (i.e., overall pooled) mean of the single-colony data, the mean of each independent experiment is shown using circles. The independent experimental means for each genotype were used for the statistical comparisons as described in Lord *et al.* (Lord *et al.*, 2020). Designations of significance are indicated in the figure legends.

Statistical analysis

For any dataset with statistics displayed, a Shapiro-Wilk test was performed to determine normality (alpha = 0.05). For parametric data, an unpaired *t* test or a one-way ordinary ANOVA with Dunnett's multiple comparisons was performed as indicated in the figure legend. For nonparametric data, a Kruskal-Wallis test with Dunn's multiple comparisons test was performed as indicated in the figure legend.

ACKNOWLEDGMENTS

We thank the past and present Lackner lab members for scientific discussions, ideas, and helpful feedback. Special thanks to Erica Rosario for assisting with data visualization and Kaylee Gonzalez for assisting with yeast strain construction. We also thank Northwestern's Cell Biology Supergroup, the Wignall-Lackner (WiLa) Cell Biology Group, and the Biotechnology Training Program for suggestions and feedback. Thank you to the Brickner lab for providing yeast strains and plasmids. All microscopy was performed at the Biological Imaging Facility at Northwestern University (RRID:SCR_017767), supported by the Chemistry for Life Processes Institute, the Northwestern University Office for Research, the Department of Molecular Biosciences, and the Rice Foundation. Special thanks to Jessica Hornick and Tong Zhang for assistance with microscopy. C.S.H. was supported by National Institutes of Health Biotechnology Training Program 5T32GM008449-25 and National Science Foundation Graduate Research Fellowship Program under Grant No. DGE-1842165. J.C.C is supported by National Institutes of Health, National Institute of General Medical Sciences grant 1F32GM145160-01. L.L.L. is supported by National Institutes of Health, National Institute of General Medicine Sciences grant R01GM120303.

REFERENCES

Abrisch RG, Gumbin SC, Wisniewski BT, Lackner LL, Voeltz GK (2020). Fission and fusion machineries converge at ER contact sites to regulate mitochondrial morphology. J Cell Biol 219, e201911122.

Adames NR, Cooper JA (2000). Microtubule interactions with the cell cortex causing nuclear movements in Saccharomyces cerevisiae. J Cell Biol 149, 863–874.

Amado L, Cogan AP, González Montoro A (2023). Different tether proteins of the same membrane contact site affect the localization and mobility of each other. J Cell Sci 136, jcs260786.

Benedetti L (2021). Optogenetic Tools for Manipulating Protein Subcellular Localization and Intracellular Signaling at. Organelle Contact Sites. Curr Protoc 1, e71.

Booth DM, Enyedi B, Geiszt M, Várnai P, Hajnóczky G (2016). Redox Nanodomains Are Induced by and Control Calcium Signaling at the ER-Mitochondrial Interface. Mol Cell 63, 240–248.

Booth DM, Várnai P, Joseph SK, Hajnóczky G (2021). Oxidative bursts of single mitochondria mediate retrograde signaling toward the ER. Mol Cell 81, 3866–3876.e2.

Carminati JL, Stearns T (1997). Microtubules orient the mitotic spindle in yeast through dynein-dependent interactions with the cell cortex. J Cell Biol 138, 629–641.

Cerveny KL, Jensen RE (2003). The WD-repeats of Net2p interact with Dnm1p and Fis1p to regulate division of mitochondria. Mol Biol Cell 14, 4126–4139.

Cerveny KL, McCaffery JM, Jensen RE (2001). Division of mitochondria requires a novel DNM1-interacting protein, Net2p. Mol Biol Cell 12, 309–321.

Cerveny KL, Studer SL, Jensen RE, Sesaki H (2007). Yeast mitochondrial division and distribution require the cortical Num1 protein. Dev Cell 12, 363–375.

Chao JT, Wong AKO, Tavassoli S, Young BP, Chruscicki A, Fang NN, Howe LJ, Mayor T, Foster LJ, Loewen CJR (2014). Polarization of the endoplasmic reticulum by ER-septin tethering. Cell 158, 620–632.

Chen S, Novick P, Ferro-Novick S (2012). ER network formation requires a balance of the dynamin-like GTPase Sey1p and the Lunapark family member Lnp1p. Nat Cell Biol 14, 707–716.

Csordás G, Várnai P, Golenár T, Roy S, Purkins G, Schneider TG, Balla T, Hajnóczky G (2010). Imaging interorganelle contacts and local calcium dynamics at the ER-mitochondrial interface. Mol Cell 39, 121–132.

David Y, Castro IG, Schuldiner M (2021). The Fast and the Furious: Golgi Contact Sites. Contact 4, 1–15.

Eisenberg-Bord M, Shai N, Schuldiner M, Bohnert M (2016). A Tether Is a Tether Is a Tether: Tethering at Membrane Contact Sites. Dev Cell 39, 395–409.

Eshel D, Urrestarazu LA, Vissers S, Jauniaux JC, van Vliet-Reedijk JC, Planta RJ, Gibbons IR (1993). Cytoplasmic dynein is required for normal nuclear segregation in yeast. Proc Natl Acad Sci USA 90, 11172–11176.

Eves PT, Jin Y, Brunner M, Weisman LS (2012). Overlap of cargo binding sites on myosin V coordinates the inheritance of diverse cargoes. J Cell Biol 198, 69–85.
Fagarasanu A, Rachubinski RA (2007). Orchestrating organelle inheritance in Saccharomyces cerevisiae. Curr Opin Microbiol 10, 528–538.
Farkasovsky M, Küntzel H (1995). Yeast Num1p associates with the mother cell cortex during S/G2 phase and affects microtubular functions. J Cell Biol 131, 1003–1014.
Farkasovsky M, Küntzel H (2001). Cortical Num1p interacts with the dynein intermediate chain Pac11p and cytoplasmic microtubules in budding yeast. J Cell Biol 152, 251–262.
Geissmann Q (2013). OpenCFU, a new free and open-source software to count cell colonies and other circular objects. PLoS One 8, e54072.
Gruber S, Arumugam P, Katou Y, Kuglitsch D, Helmhart W, Shirahige K, Nasmyth K (2006). Evidence that loading of cohesin onto chromosomes involves opening of its SMC hinge. Cell 127, 523–537.
Hammermeister M, Schödel K, Westermann B (2010). Mdm36 is a mitochondrial fission-promoting protein in Saccharomyces cerevisiae. Mol Biol Cell 21, 2443–2452.
Harper CS, White AJ, Lackner LL (2020). The multifunctional nature of mitochondrial contact site proteins. Curr Opin Cell Biol 65, 58–65.
Haruki H, Nishikawa J, Laemmli UK (2008). The anchor-away technique: rapid, conditional establishment of yeast mutant phenotypes. Mol Cell 31, 925–932.
Heil-Chapdelaine RA, Oberle JR, Cooper JA (2000). The cortical protein Num1p is essential for dynein-dependent interactions of microtubules with the cortex. J Cell Biol 151, 1337–1344.
Hoppins S, Lackner L, Nunnari J (2007). The machines that divide and fuse mitochondria. Annu Rev Biochem 76, 751–780.
Janke C, *et al*. (2004). A versatile toolbox for PCR-based tagging of yeast genes: new fluorescent proteins, more markers and promoter substitution cassettes. Yeast 21, 947–962.
Katona M, Bartók Á, Nichtova Z, Csordás G, Berezhnaya E, Weaver D, Ghosh A, Várnai P, Yule DI, Hajnóczky G (2022). Capture at the ER-mitochondrial contacts licenses IP3 receptors to stimulate local Ca2+ transfer and oxidative metabolism. Nat Commun 13, 6779.
Klecker T, Scholz D, Förtsch J, Westermann B (2013). The yeast cell cortical protein Num1 integrates mitochondrial dynamics into cellular architecture. J Cell Sci 126, 2924–2930.
Knoblach B, Rachubinski RA (2015). Sharing the cell's bounty - organelle inheritance in yeast. J Cell Sci 128, 621–630.
Kormanec J, Schaaff-Gerstenschläger I, Zimmermann FK, Perecko D, Küntzel H (1991). Nuclear migration in Saccharomyces cerevisiae is controlled by the highly repetitive 313 kDa NUM1 protein. Mol Gen Genet 230, 277–287.
Kraft LM, Lackner LL (2017). Mitochondria-driven assembly of a cortical anchor for mitochondria and dynein. J Cell Biol 216, 3061–3071.
Kraft LM, Lackner LL (2019). A conserved mechanism for mitochondria-dependent dynein anchoring. Mol Biol Cell 30, 691–702.
Kwak C, *et al*. (2020). Contact-ID, a tool for profiling organelle contact sites, reveals regulatory proteins of mitochondrial-associated membrane formation. Proc Natl Acad Sci USA 117, 12109–12120.
Lackner LL (2019). The Expanding and Unexpected Functions of Mitochondria Contact Sites. Trends Cell Biol 29, 580–590.
Lackner LL, Horner JS, Nunnari J (2009). Mechanistic analysis of a dynamin effector. Science 325, 874–877.
Lackner LL, Nunnari JM (2009). The molecular mechanism and cellular functions of mitochondrial division. Biochim Biophys Acta 1792, 1138–1144.
Lackner LL, Ping H, Graef M, Murley A, Nunnari J (2013). Endoplasmic reticulum-associated mitochondria-cortex tether functions in the distribution and inheritance of mitochondria. Proc Natl Acad Sci USA 110, E458–E467.
Lammers LG, Markus SM (2015). The dynein cortical anchor Num1 activates dynein motility by relieving Pac1/LIS1-mediated inhibition. J Cell Biol 211, 309–322.
Li KW, Lu MS, Iwamoto Y, Drubin DG, Pedersen RTA (2021). A preferred sequence for organelle inheritance during polarized cell growth. J Cell Sci 134, jcs258856.
Longtine MS, McKenzie A 3rd, Demarini DJ, Shah NG, Wach A, Brachat A, Philippsen P, Pringle JR (1998). Additional modules for versatile and economical PCR-based gene deletion and modification in Saccharomyces cerevisiae. Yeast 14, 953–961.
Lord SJ, Velle KB, Mullins RD, Fritz-Laylin LK (2020). SuperPlots: Communicating reproducibility and variability in cell biology. J Cell Biol 219, e202001064.
Mahecic D, Carlini L, Kleele T, Colom A, Goujon A, Matile S, Roux A, Manley S (2021). Mitochondrial membrane tension governs fission. Cell Rep 35, 108947.
Mears JA, Lackner LL, Fang S, Ingerman E, Nunnari J, Hinshaw JE (2011). Conformational changes in Dnm1 support a contractile mechanism for mitochondrial fission. Nat Struct Mol Biol 18, 20–26.
Miller RK, Rose MD (1998). Kar9p is a novel cortical protein required for cytoplasmic microtubule orientation in yeast. J Cell Biol 140, 377–390.
Morawska M, Ulrich HD (2013). An expanded tool kit for the auxin-inducible degron system in budding yeast. Yeast 30, 341–351.
Mozdy AD, McCaffery JM, Shaw JM (2000). Dnm1p GTPase-mediated mitochondrial fission is a multi-step process requiring the novel integral membrane component Fis1p. J Cell Biol 151, 367–380.
Naylor K, Ingerman E, Okreglak V, Marino M, Hinshaw JE, Nunnari J (2006). Mdv1 interacts with assembled Dnm1 to promote mitochondrial division. J Biol Chem 281, 2177–2183.
Nishimura K, Fukagawa T, Takisawa H, Kakimoto T, Kanemak M (2009). An auxin-based degron system for the rapid depletion of proteins in non-plant cells. Nat Methods 6, 917–922.
Nunnari J, Suomalainen A (2012). Mitochondria: in sickness and in health. Cell 148, 1145–1159.
Omer S, Greenberg SR, Lee W-L (2018). Cortical dynein pulling mechanism is regulated by differentially targeted attachment molecule Num1. Elife 7, e36745.
Osman C, Noriega TR, Okreglak V, Fung JC, Walter P (2015). Integrity of the yeast mitochondrial genome, but not its distribution and inheritance, relies on mitochondrial fission and fusion. Proc Natl Acad Sci USA 112, E947–E956.
Ping HA, Kraft LM, Chen W, Nilles AE, Lackner LL (2016). Num1 anchors mitochondria to the plasma membrane via two domains with different lipid binding specificities. J Cell Biol 213, 513–524.
Prinz WA, Toulmay A, Balla T (2020). The functional universe of membrane contact sites. Nat Rev Mol Cell Biol 21, 7–24.
Roux A, Uyhazi K, Frost A, De Camilli P (2006). GTP-dependent twisting of dynamin implicates constriction and tension in membrane fission. Nature 441, 528–531.
Schauss AC, Bewersdorf J, Jakobs S (2006). Fis1p and Caf4p, but not Mdv1p, determine the polar localization of Dnm1p clusters on the mitochondrial surface. J Cell Sci 119, 3098–3106.
Schauss AC, McBride HM (2007). Mitochondrial Fission: A Non-Nuclear Role for Num1p. Curr Biol 17, R467–R470.
Schmit HL, Kraft LM, Lee-Smith CF, Lackner LL (2018). The role of mitochondria in anchoring dynein to the cell cortex extends beyond clustering the anchor protein. Cell Cycle 17, 1345–1357.
Scorrano L, *et al*. (2019). Coming together to define membrane contact sites. Nat Commun 10, 1287.
Sesaki H, Jensen RE (1999). Division versus fusion: Dnm1p and Fzo1p antagonistically regulate mitochondrial shape. J Cell Biol 147, 699–706.
Sheff MA, Thorn KS (2004). Optimized cassettes for fluorescent protein tagging in Saccharomyces cerevisiae. Yeast 21, 661–670.
Tang X, Germain BS, Lee W-L (2012). A novel patch assembly domain in Num1 mediates dynein anchoring at the cortex during spindle positioning. J Cell Biol 196, 743–756.
Tang X, Punch JJ, Lee W-L (2009). A CAAX motif can compensate for the PH domain of Num1 for cortical dynein attachment. Cell Cycle 8, 3182–3190.
Tieu Q, Nunnari J (2000). Mdv1p is a WD repeat protein that interacts with the dynamin-related GTPase, Dnm1p, to trigger mitochondrial division. J Cell Biol 151, 353–366.
Tieu Q, Okreglak V, Naylor K, Nunnari J (2002). The WD repeat protein, Mdv1p, functions as a molecular adaptor by interacting with Dnm1p and Fis1p during mitochondrial fission. J Cell Biol 158, 445–452.
Walther TC, Brickner JH, Aguilar PS, Bernales S, Pantoja C, Walter P (2006). Eisosomes mark static sites of endocytosis. Nature 439, 998–1003.
White AJ, Harper CS, Rosario EM, Dietz JV, Addis HG, Fox JL, Khalimonchuk O, Lackner LL (2022). Loss of Num1-mediated cortical dynein anchoring negatively impacts respiratory growth. J Cell Sci 135, jcs259980.
Yu JW, Mendrola JM, Audhya A, Singh S, Keleti D, DeWald DB, Murray D, Emr SD, Lemmon MA (2004). Genome-wide analysis of membrane targeting by S. cerevisiae pleckstrin homology domains. Mol Cell 13, 677–688.
Zhang Y, Chan DC (2007). Structural basis for recruitment of mitochondrial fission complexes by Fis1. Proc Natl Acad Sci USA 104, 18526–18530.